Quaternary Science Reviews 377 (2026) 109838

Contents lists available at ScienceDirect

Quaternary Science Reviews

journal homepage: www.elsevier.com/locate/quascirev

A paleoclimate reference record spanning the last 1 million years from the Fram Strait (Sites U1621 and U1623, IODP Expedition 403)

A. González-Lanchas [a,*], B.T. Reilly [b], M.A. Bárcena [c], S. De Schepper [d], A.C. Gebhardt [e], J. Gruetzner [e], K. Husum [f], Y. Rosenthal [g], Y. Suganuma [h], Y. Zhong [i], R.E.M. Rickaby [a], A.K.I.U. Kapuge [j], L.R. Monito [k], J. Yeon [l], R.G. Lucchi [m], K. St. John [n], T.A. Ronge [l], L. Duxbury [o], G. Goss [p], N. Greco [q], L. Haygood [r], M. Iizuka [s], A.R. Lam [t], O. Libman-Roshal [u], Y. Liu [v], Y. Sakai [w], A.V. Sijinkumar [x]

[a] Department of Earth Sciences, University of Oxford, Oxford, United Kingdom
[b] Lamont-Doherty Earth Observatory, Columbia University, Palisades, NY, USA
[c] Department of Geology, University of Salamanca, Salamanca, Spain
[d] NORCE Research and Bjerknes Centre for Climate Research, University of Bergen, Bergen, Norway
[e] Alfred Wegener Institute, Helmholtz Center for Polar and Marine Research, Bremerhaven, Germany
[f] Norwegian Polar Institute, Tromsø, Norway
[g] Institute of Marine and Coastal Sciences, Rutgers University, New Brunswick, USA
[h] National Institute of Polar Research, Tachikawa, Tokyo, Japan
[i] Advanced Institute of Ocean Research, Southern University of Science and Technology, Shenzhen, 518055, China
[j] Department of Earth Sciences, University of Delaware, Newark, DE, USA
[k] Department of Geological Sciences, University of Florida, Gainesville, USA
[l] Texas A&M University, College Station, USA
[m] Istituto Nazionale di Oceanografia e di Geofisica Sperimentale, Trieste, Italy
[n] Department of Geology and Environmental Science, James Madison University, Harrisonburg, USA
[o] Institute for Marine and Antarctic Studies, Tasmania, Australia
[p] Department of Earth and Planetary Sciences, Yale University, New Haven, USA
[q] National Center for Ecological Analysis and Synthesis, University of California, Santa Barbara, USA
[r] Boone Pickens School of Geology, Oklahoma State University, Stillwater, USA
[s] Geological Survey of Japan, National Institute of Advanced Industrial Science and Technology, Tsukuba, Japan
[t] Earth Sciences Department, Binghamton University, Binghamton, USA
[u] Earth and Environmental Studies, Montclair State University, Montclair, USA
[v] Key Laboratory of Marine Geology and Metallogeny, First Institute of Oceanography, Ministry of Natural Resources, Qingdao, 266061, China
[w] Kyoto University Graduate School of Engineering, Kyoto, Japan
[x] Department of Geology, Central University of Kerala, Kerala, India

ARTICLE INFO

Handling Editor: Dr Mira Matthews

Keywords:
Arctic
Fram strait
Calcareous nannofossils
Magnetostratigraphy
X-ray fluorescence
Interglacials
Pleistocene
Mid-Brunhes
Mid-Pleistocene Transition
Paleoclimatology

ABSTRACT

As the main gateway to the Arctic Ocean, the Fram Strait (FS) plays a critical role in regulating central Arctic–Atlantic water exchange and global climate dynamics. Paleoclimate reconstructions from this key region remain particularly challenging due to the scarcity of continuous, well-positioned and high-resolution sedimentary records. During International Ocean Discovery Program (IODP) Expedition 403 (Eastern Fram Strait Paleo-Archive), Sites U1621 and U1623 were cored in the Bellsund Drift, southeastern Fram Strait. This study presents detailed calcareous nannofossil data from Holes U1621A and U1623A, documenting an unprecedented record of key Quaternary calcifying phytoplankton groups in the region. Intercalibrated with shipboard magnetostratigraphic data, these records establish the first chronological framework for the Bellsund Drift sediments, spanning the last ~1 million years. Increases in nannofossil abundances—defined as Nannofossil Abundance (NA) events—are identified at both sites and closely correlate with peak enhancements in Ca/Ti and Sr/Ti ratios recorded in X-ray fluorescence (XRF) data. This biogenic-geochemical covariance provides compelling evidence of fluctuations in primary productivity and sedimentary calcium carbonate ($CaCO_3$) concentration, linked to

* Corresponding author.
E-mail address: alba.gonzalez-lanchas@earth.ox.ac.uk (A. González-Lanchas).

https://doi.org/10.1016/j.quascirev.2026.109838
Received 18 October 2025; Received in revised form 21 January 2026; Accepted 22 January 2026
Available online 5 February 2026

orbitally driven changes in local conditions across glacial–interglacial (G/IG) cycles. These signals likely reflect ecological variability driven by changes in North Atlantic water inflow along the Fram Strait. The timing and structure of NA events show strong similarities with records from the palaeoceanographically connected lower-latitude Norwegian Seas. Within the structure of our record, we identify evidence of key transitions during the Pleistocene, the Mid-Pleistocene Transition (MPT) and the Mid-Brunhes Event (MBE), as well as the evolution of the interglacial phases Marine Isotope Stages (MIS) 31, 19, 15–9, 5 and the Holocene. Globally recognizable features, such as the increased pelagic production during the mid-Brunhes interval, are also observed. This study underscores the exceptional value of the Bellsund Drift as providing high-resolution records for the reconstruction of orbital scale paleoceanographic and paleoclimate variability from the key Fram Strait region during the last ~1 million years.

1. Introduction

The Arctic Ocean is undergoing rapid changes due to anthropogenic impacts on the environment (IPCC et al., 2023). Driven by "Arctic Amplification" processes, environmental changes in the Arctic appear to be accelerating (e.g., Lawrence et al., 2008; Serreze et al., 2009; Shu et al., 2022). Historical records lack sufficient temporal length to fully capture the range of potential natural variability, thus necessitating reliance on geological archives. Those records indicate that the Arctic has undergone relatively rapid climate and environmental changes in the past (e.g., Miller et al., 2010), albeit these occurred over much longer timescales (i.e., thousands of years) compared to the rapid changes observed in recent decades. Our overall understanding of the Arctic's climate history and its interactions with the global ocean system remains limited compared to other regions on Earth. This knowledge gap is chiefly due to the scarcity of continuous and well-preserved sedimentary records that enable high-resolution paleoclimate reconstructions, combined with difficulties in establishing robust and precise chronologies for the available archives.

Establishing reliable chronologies for Quaternary Arctic sediments remains a major obstacle to aligning regional paleoceanographic and paleoclimate records with global glacial-interglacial (G/IG) cycles. Decades of debate over Arctic age models reflect the persistent limitations of key stratigraphic tools (e.g., Backman et al., 2004; Hillaire-Marcel et al., 2017; Knies et al., 2025). Paleomagnetic records are often complex and ambiguous, with central Arctic records typically showing more reversals than expected based on the geomagnetic polarity timescale (e.g., O'Regan et al., 2008; Wiers et al., 2019; Witte and Kent, 1988; Xuan et al., 2012). Biostratigraphy is limited by the sporadic occurrence of stratigraphically informative microfossils. These factors have significantly constrained the identification of necessary features (i.e., standard magnetic reversals and calibrated bioevents) for the development of age models in the region (e.g., Alexanderson et al., 2014; Backman et al., 2004). Calcareous nannofossils—calcium carbonate ($CaCO_3$) scales produced by calcifying phytoplankton that are preserved in sediments—are widely used as a biostratigraphic tool in marine records (see Raffi and Backman, 2022 and references therein). Their utility stems from the rapid evolution of calcifying phytoplankton groups since the Late Triassic (Bown, 1998), with species appearances and disappearances (i.e., lowest occurrence, LO, and highest occurrence, HO, respectively) represented in sediments, serving as key biostratigraphic horizons. Applying this framework in the Arctic is particularly challenging. The cold conditions in the high latitudes severely restrict the presence of calcifying phytoplankton, resulting in low-diversity communities and the representation of discontinuous nannofossil assemblages in sediments (e.g., Nowaczyk and Baumann, 1992; O'Regan et al., 2020; Razmjooei et al., 2023).

International Ocean Discovery Program (IODP) Expedition 403 aimed to enhance our understanding of the roles played by the North Atlantic and Arctic Oceans in the climatic evolution of the Northern Hemisphere through drilling on the western continental margin of the Svalbard archipelago, located in the eastern Fram Strait (FS; Lucchi et al., 2026; Fig. 1). This area is crucial for the northward flow of warm Atlantic waters into the Arctic Ocean and is highly sensitive to climatic variability (Rudels et al., 2000). On geological timescales, the record of past interglacial stages in this area could provide useful analogues to recent changes under a range of radiative forcing. Additionally, record of the variability of the marine-based paleo-Svalbard Barents Sea Ice Sheet (SBSIS) during past glacial times could provide a unique framework for studying the modern West Antarctic Ice Sheet (Lucchi et al., 2026). Consequently, the eastern FS represents a key location for investigating past interactions among the ocean, climate, and cryosphere.

Recovering expanded and datable sedimentary successions from the Bellsund Drift, in the southeastern sector of the FS, Sites U1621 and U1623 (Fig. 1) represent promising archives for understanding oceanographic and ice sheet evolution in the region during the Quaternary. Sites U1621 and U1623 benefit from high core recovery, particularly in piston cored sediments, and the construction of a stratigraphic splice to ensure the complete capture of the sedimentary sucessions (Lucchi et al., 2026). Their relatively southerly position, direct exposure to warm Atlantic water inflow, and proximity to the paleo–SBSIS, enhance their suitability for detailed paleoclimatic and paleoceanographic analyses. In addition, these locations have been already assesed to have the potential to preserve thick interglacial deposits, as demonstrated by the ~6 m Holocene interval recovered in site survey Core GS191-01 PC (Caricchi et al., 2019). .

We present unprecendented calcareous nannofossil records from Bellsund Drift Sites U1621 and U1623 (Fig. 1). These records capture evidence of the lineage evolution of the Noelaerhabdaceae family, the dominant calcifying phytoplankton group throughout the Quaternary. Intercalibrated with magnetostratigraphy, our analysis establishes a first detailed chronostratigraphy for these sites spanning the last ~1 million years. Integrated with X-ray fluorescence (XRF)-derived Ca/Ti and Sr/Ti profiles from Site U1623, the nannofossil abundance (NA) events defined in this study are interpreted to reflect orbital-scale paleoceanographic variability associated with G/IG cycles and major Pleistocene paleoclimate transitions at the FS. This contribution highlights the significance of the Bellsund Drift sedimentary successions as high-latitude reference records for high-resolution paleoclimate investigation in future research.

2. Modern oceanography and surface production setting

The surface oceanography of the eastern FS is primarily influenced by the northward flow of the West Spitsbergen Current (WSC), the northernmost extension of the North Atlantic Current (NAC) that transports relatively warm and saline waters of Atlantic origin (Walczowski and Piechura, 2011; Fig. 1). Before entering the Arctic Ocean, the WSC follows the western continental margin of Spitsbergen (i.e., Svalbard archipielago; Blindheim and Osterhus, 2005), where its interaction with the seafloor leads to the formation of a series of mounded depocenters (i.e., sediment drifts), through sediment transport and deposition along the Svalbard margin (Fig. 1). The northward flow of North Atlantic water (i.e., hereafter referred to as NAW) along these currents, plays a fundamental role in delivering heat and moisture toward Arctic latitudes, thereby reducing sea-ice extent across the Norwegian, Barents, and Greenland Seas (i.e., the Nordic Seas) and the

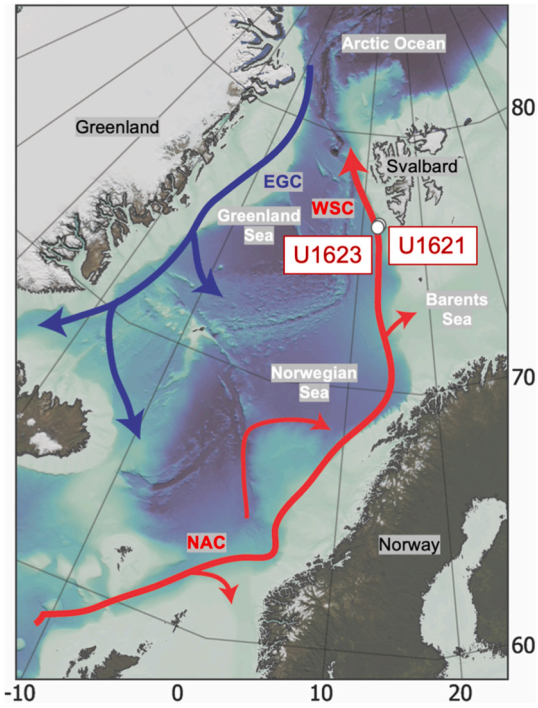

Fig. 1. Location of IODP Sites U1621 and U1623 in the southeastern Fram Strait (FS) and schematic representation of the oceanographic currents in the region. WSC: West Spitsbergen Current; EGC: Eastern Greenland Current; NAC: North Atlantic Current. Land image is extracted from the Blue Marble 2004 product from the NASA Earth Observatory (Stöckli et al., 2005); bathymetry is extracted from the GEBCO 2023 Grid (GEBCO Compliation Group, 2023). (For interpretation of the references to color in this figure legend, the reader is referred to the Web version of this article.)

eastern FS (Seidov et al., 2015; Fig. 1).

Annual coccolithophore (i.e., calcifying phytoplankton) production in the Nordic seas and the southeastern FS region is primarily controlled by NAW, largely driving surface ocean temperatures, nutrient availability, and vertical mixing dynamics. In the FS, production rates are typically highest from summer to early autumn, coinciding with the seasonal intensification of the NAW (Dylmer et al., 2015). Calcifying phytoplankton peak production appears closely tied to the spatial extent of NAW and the position of the Arctic Front. This oceanic frontal system marks the boundary between cooler Polar Waters and the warmer NAW, and plays a key role in promoting vertical mixing and nutrient supply. Together, these drivers associated to NAW influence, create favorable conditions for calcifying phytoplankton proliferation (Forest et al., 2010).

3. Materials and methods

3.1. IODP sites U1621 and U1623

Sites U1621 (76°31.3152′N, 12°44.3552′E) and U1623 (76°31.8594′N, 12°34.4276′E) were cored in water depths of 1,639 m and 1,708 m, respectively, at the Bellsund Drift, located on the western margin of Svalbard, southeastern FS (Fig. 1). Recovered sediments are primarily siliciclastic silty clay, with some coarser intervals including sandy mud and diamicton (Lucchi et al., 2026).

A total of 213 samples were studied from the Bellsund Sites U1621 and U1623 for calcareous nannofossil analysis. 73 samples were taken along the working halves of Cores U1621A-1H to U1621A-28X. This corresponds to the interval between 1 and 205.92 m core depth below seafloor, method A (CSF-A), which we refer as meters below sea floor (mbsf) throughout the rest of the manuscript. This corresponds to depths between 0 and 224.52 m core composite depth below seafloor (CCSF), which we refer to as meters composite depth below seafloor (mcd) throughout the manuscript. For Site U1623, 140 samples were selected along the working halves of Cores U1623A-1H to U1623A-51X. This corresponds to the interval between 0 and 369.12 mbsf, or between 0 and 401.91 mcd. In addition to routine core catcher, supplementary samples were selected along the working halves in order to capture a variety of lithofacies. Sample selection was based on a combination of visual criteria (i.e., sediment color changes and sedimentary structures) and evaluation of shipboard profiles of physical properties (i.e., magnetic susceptibility). All samples together average a sampling spacing of ~2.85 m across sections.

A total of 41 vertically oriented paleomagnetic cube samples were taken from the working half sections of Hole U1621A, and 130 vertically oriented paleomagnetic cube samples were taken from Hole U1623A, with a sample resolution of about 1 cube per 5 m in the entirety of Hole U1621A and in the APC cored sections of Hole U1623A (i.e., about 2 cubes per APC core). Higher-resolution sampling was conducted in the XCB cored intervals of Hole U1623A that were suspected to be important for identifying polarity zones in the late Matuyama Chron (C1r; 0.773–1.775 Ma). Care was taken to sample from the centre of cores in sediments that showed little if any core disturbance, avoiding bowed sediments near core edges in APC cores and targeting larger intact biscuits in XCB cored intervals when possible.

3.2. Sample preparation and calcareous nannofossil analysis

Smear slides for calcareous nannofossil analysis were prepared from unprocessed sediments following the standard technique (e.g., Bown, 1998). Calcareous nannofossil biohorizon identification for biostratigraphic determination was based on the Lowest Occurrence (LO) and Highest Occurrence (HO) of index taxa in samples. The concentration of calcareous nannofossils was calculated based on a quantitative census covering an area over 1 mm^2 (i.e., over 25 fields of view per sample, randomly distributed throughout the slide). Additional qualitative visual field examinations were carried out to ensure accuracy in the identification of biohorizons. Microscope analysis was performed with the use of a Zeiss AXIO Imager A2 linearly polarized light microscope at magnification x1000, onboard the *JOIDES Resolution*, with complementary examination on a ZEISS Axio Scope A1 at the Department of Earth Sciences of the University of Oxford (United Kingdom). Calcareous nannofossil abundances are presented as concentration of nannofossils per field of view (FV). The relative abundances (%) of the biostratigraphic index species are also included. Nannofossil components from older stratigraphic levels of pre Neogene age (i.e., reworked nannofossils) were intermittently observed, in a variable content, at the Bellsund Drift sediments (Lucchi et al., 2026). Those specimens are not considered for nannofossil quantification and the calculation of concentrations and relative abundances presented and discussed in this study.

Taxonomic criteria for species identification followed Young et al. (2003) and the guide of coccolithophore biodiversity and taxonomy Nannotax 3 (Young et al., 2026). We followed the calcareous nannofossil bioevents and calibrations summarized in Gradstein and Ogg (2020). This considers the original definition of bioevents by Thierstein et al. (1977), Raffi et al. (2006) and Backman et al. (2012). The standard biozonation by Martini (1971) was adopted. The depth of each bioevent at Holes U1621A and U1623A was calculated as the average between the depth of the sample in which the event was recorded and that of the next shallower sample studied (HOs), or the next deeper sample (LOs). Depths are reported on the mcd depth scale unless otherwise stated.

3.3. Magnetostratigraphy

Paleomagnetic natural remanent magnetization (NRM) measurements were made on the cube samples using the *JOIDES Resolution* 2G

Enterprises superconducting rock magnetometer (SRM) equipped with inline alternating field (AF) coils. The NRM of the cube samples was subject to stepwise AF demagnetization at peak fields between 0 and 50 mT in 5 mT increments for Hole U1621A. Samples from Hole U1623A followed the same procedure, excluding the 5 and 50 mT peak AF steps. Demagnetization data and the anisotropy of magnetic susceptibility were used to assess the stability of the NRM, the extent of the magnetization imparted by the drill string, and the preservation of the sedimentary fabric (Lucchi et al., 2026).

In general, both Sites U1621 and U1623 hosted reliable magnetizations (Lucchi et al., 2026), and following the assessment described above, interpretations for this study are based on data from 40 of the 41 samples taken from Site U1621 and 126 of the 130 paleomagnetic samples taken from Site U1623. The magnetostratigraphic interpretation in this paper is based on inclination values measured after 30 mT peak AF demagnetization.

3.4. X-ray fluorescence (XRF) analysis

Sediments from Site U1623 were scanned at Texas A&M University's Gulf Coast Repository (USA), using a third-generation Avaatech X-ray fluorescence (XRF) core scanner, which utilizes Energy Dispersive Spectroscopy (EDS). This instrument is equipped with a 100 W Oxford X-ray tube and a BrightSpec TopazX multichannel analyzer with a silicon drift detector (SDD). The scanner's cross and downcore window slits were set to 12 and 10 mm, respectively. The archive half sections were scanned at 5 cm at 10 and 30 kV excitation level, which encompasses most major, minor, and geologically relevant trace elements. The 10 kV scan did not utilize any filter, while the 30 kV utilized the Pd-thick filter. Due to disturbed intervals, or the presence of dropstones, biscuiting, or voids, certain core sections were scanned at irregular intervals. These intervals were specifically chosen to have smooth surfaces better suited for XRF data collection. As a result, some portions of the XRF record contain data gaps. To ensure optimal detector placement and to avoid unsuitable areas, a 3D-printed replica of the scanner window was used to identify appropriate scanning positions.

Quality control was ensured by analyzing internal laboratory instrument standards at the beginning and end of each scanning day, as well as by maintaining a constant helium purge through the enclosed detector prism housing to ensure consistency in throughput values throughout the scanning sessions. Furthermore, all datapoints that had positive Argon values were excluded from our interpretations as the presence of argon indicates that the scanner's detector did not sit flush on the section's surface or measured a void, and thus recorded ambient air which decreases the quality of the data.

The XRF data are presented on a continuous splice constructed during Expedition 403. The upper 29.73 mcd uses data from the alternate splice, while below this depth, all data are from the primary splice (Lucchi et al., 2026). XRF data are smoothed using a 1 m full-width at half-maximum Gaussian filter. The elemental ratios of Ca/Ti and Sr/Ti are used to reconstruct relative variations in carbonate versus siliciclastic sediment input. Ca reflects both biogenic and detrital carbonate, whereas Sr is more specifically linked to pelagic biogenic $CaCO_3$, as primary calcifyiers (e.g., calcifying phytoplankton and foraminifera) incorporate more Sr (i.e., Hodell et al., 2008; Jackson et al., 2023). Therefore, while both profiles allow constraining $CaCO_3$ to siliciclastic content, Sr/Ti is a more sensitive proxy to characterize biogenic $CaCO_3$ concentration in sediments. Profiles are presented as logarithmic ratio, ln(Ca/Ti) and ln(Sr/Ti).

4. Results

4.1. Nannofossil abundance structure

The representation and concentration of calcareous nannofossils in sediments at both Holes U1621A and U1623A are characterized by intervals of peak structure, with a variable nannofossil concentrations, alternating with barren sections (Figs. 2 and 3).

Calcareous nannofossil peak abundances at the Bellsund drift records are defined as Nannofossil Abundance events (NA), a term introduced in this study. These features are numbered as NA1 to 11 in Hole U1621A and as NA1 to 16 in Hole U1623A (Figs. 2 and 3). The top and base depths of each NA event are determined by averaging the depth of the last sample in which the NA is observed and that of the next shallower or deeper studied sample. A complete list of the NA events for Sites U1621 and U1623, including their top and base depths for each site, is provided in the Supplementary Table 1.

Across Hole U1621A, more continuous and prominent NA events are recorded in the upper 32.64 m (0–32.64 mcd) and between 86.53 and 150.43 mcd (i.e., NA1 to 2 and NA5 to 9, respectively; Fig. 2 and Table S1). The NA5 event at Hole U1621A, centred at 91.95 mcd, is characterized by the highest nannofossil concentrations of this record. At Hole U1623A, more continuous and prominent NA events are recorded in the upper 18.92 m (0–18.92 mcd) and between 66.17 and 312.05 mcd (i.e., NA1 to 2 and NA4 to 16; Fig. 3 and Table S1). The NA5 to NA8 events, recorded between 96.68 and 112.40 mcd, are characterized by the highest nannofossil concentrations in this hole (Fig. 3 and Table S1). Both Holes U1621A and U1623A show intervals with markedly reduced, or absent, calcareous nannofossil representation in samples between 36.81 and 83.37 mcd, at Hole U1621A (i.e., NA3 to NA4; Fig. 2 and Table S1) and between 23.64 and 66.17 mcd, at U1623A (i.e., NA3; Fig. 3 and Table S1). Intervals with reduced nannofossil abundance, or absence, are similarly observed in the lowermost sections of both records; below 150.43 mcd at Hole U1621A (i.e., NA 10 to 11; Fig. 2 and Table S1), and below 312.05 mcd at Hole U1623A (Fig. 3).

4.2. Composition of nannofossil assemblages

A total of 9 taxa groups were identified in the samples from Holes U1621A and U1623A. These include *Emiliania huxleyi*, small *Gephyrocapsa* species, *Gephyrocapsa caribbeanica*, *Gephyrocapsa muellerae, Pseudoemiliania lacunosa*, *Reticulofenestra asanoi*, *Coccolithus pelagicus*, *Calcidiscus leptoporus*, and *Helicosphaera carteri*. The *Gephyrocapsa*, *Pseudoemiliania* and *Reticulofenestra* spp. species all belong to family Noelaerhabdaceae. Note that *E. huxleyi* has been formally redefined within the *Gephyrocapsa* genus as (i.e., *G. huxleyi*, by Bendif et al. 2023); here we retain the more common terminology. Specimens within family Noelaerhabdaceae constitute the dominant component of the nannofossil assemblages at both Holes U1621A and U1623A (Figs. 2 and 3). While the assemblage representation is not cointinuous along samples, the succession of Noelaerhabdaceae specimens across the Sites U1621 and U1623 records (Figs. 2 and 3) alignes well with the lineage evolution of this family (e.g., Bown, 1998; Young et al., 2003; Young et al., 2026). The sedimentary record of this lineage (i.e., calibrated LO and HOs) has been widely used as a biostratigraphic tool across the Quaternary (e.g., Raffi et al., 2006; Thierstein et al., 1977; Wei, 1993). The species *E. huxleyi*, *G. caribbeanica, P. lacunosa* and *R. asanoi* are biostratigraphically useful and provide the basis for biochronological determination in this study (Figs. 2 and 3). Small *Gephyrocapsa* and *G. muellerae* are consistently present in assemblages at both Holes U1621A and Hole U1623A. These do not provide biostratigraphic information but their abundances are included in the nannofossil concentration values (Figs. 2 and 3). The ecological value of Noelaerhabdaceae specimens is considered and lately discussed for the interpretation of paleoceanographically-driven environmental variability in the FS.

At Hole U1621A, the species *E. huxleyi* is identified in continuity above 54.2 mcd, with a scarce representation of specimens observed in one sample at 73.9 mcd (Fig. 2). The interval between 72.37 and 159.97 mcd is characterized by the presence of *G. caribbeanica* (Fig. 2). The species *P. lacunosa* is observed in only one sample at 191.43 mcd (Fig. 2).

At Hole U1623A, representation of *E. huxleyi* is observed from 28.23

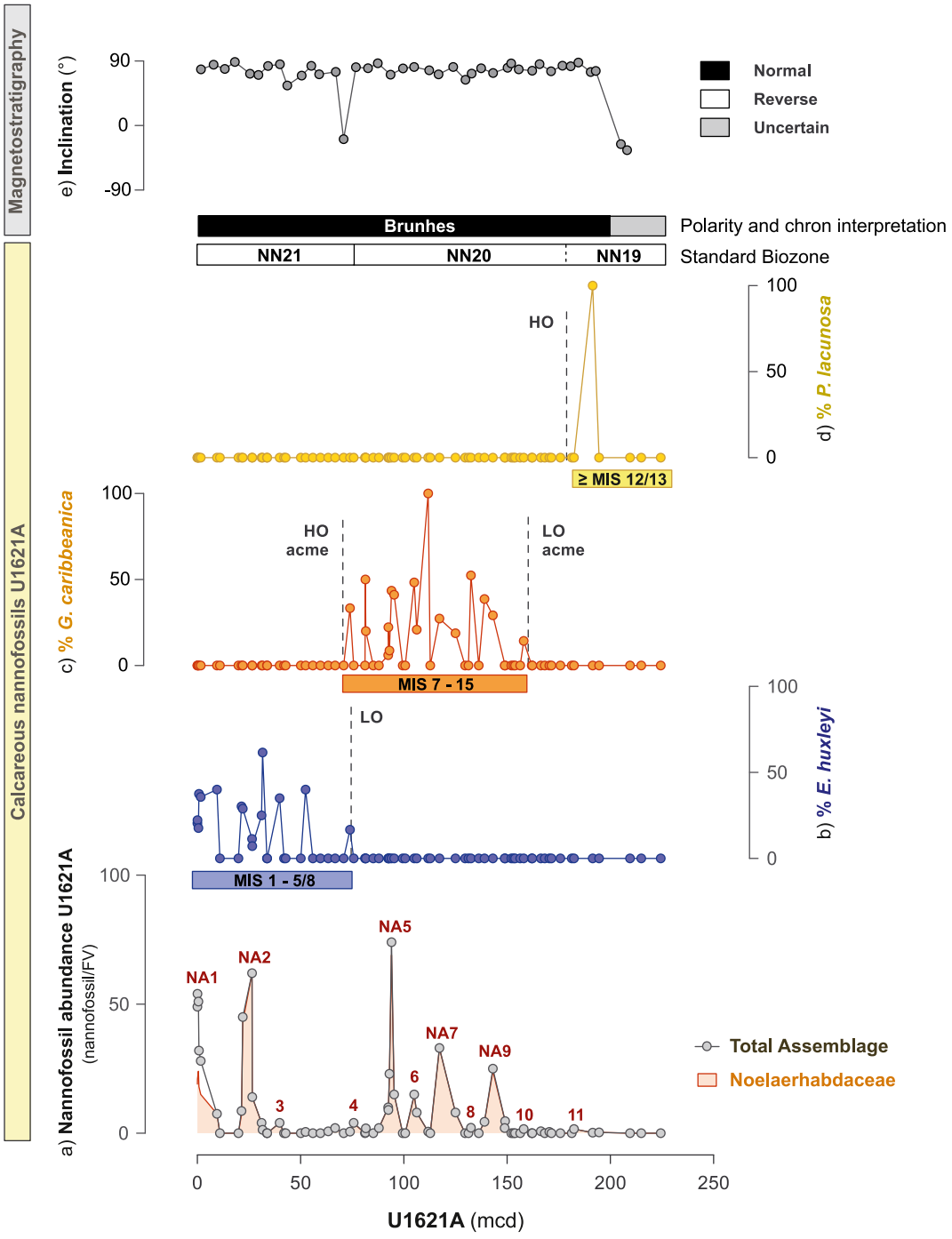

Fig. 2. Calcareous nannofossil content, biostratigraphic scheme, magnetostratigraphic inclination data and polarity definition at Hole U1621A. **a)** Concentration of nannofossils in samples (per field of view; FV); Representation of the total assemblage (grey line) and Noelaerhabdaceae specimens (filled with orange). Nannofossil abundance events (NA1 to 11) are labeled. Percent abundances (%) of biostratigraphic index species: **b)** % *Emiliania huxleyi*; **c)** % *Gephyrocapsa caribbeanica*; **d)** % *Pseudoemiliania lacunosa*. **e)** Paleomagnetic inclination after 30 mT peak AF demagnetization. LO = Lowest Occurrence; HO = Highest Occurrence. The lower bars indicate Marine Isotope Stages (MIS), according to Lisiecki and Raymo, 2005, and determined by the presence of biostratigraphic index species. Summarized calcareous nannofossil biozonation (Martini 1971) and polarity interpretation and chron identification (Gradstein and Ogg, 2020) are included. A list of calcareous nannofossil biohorizons at Hole U1621A and their mbsf and mcd depths is includded in Supplementary Table S2. (For interpretation of the references to color in this figure legend, the reader is referred to the Web version of this article.)

mcd to the top of the section (Fig. 3). The interval between 62.06 and 167.76 mcd is characterized by the presence of *G. caribbeanica* (Fig. 3). At this hole, the species *P. lacunosa* is recorded below 153.55 mcd (Fig. 3). Below that depth, the lowermost section at Hole U1623A is characterized by the presence of specimens belonging to *R. asanoi*, identified between 164.71 and 307.78 mcd. Among these taxa, specimens with sizes >6 μm are identified between 221.83 and 307.78 mcd (Fig. 3).

4.3. Magnetic inclinations and polarity definition

Sites U1621 and U1623 are located at high northern latitudes, around 76.5° N, and thus are expected to host steep and positive (or negative) inclination during times of normal (or reverse) polarity.

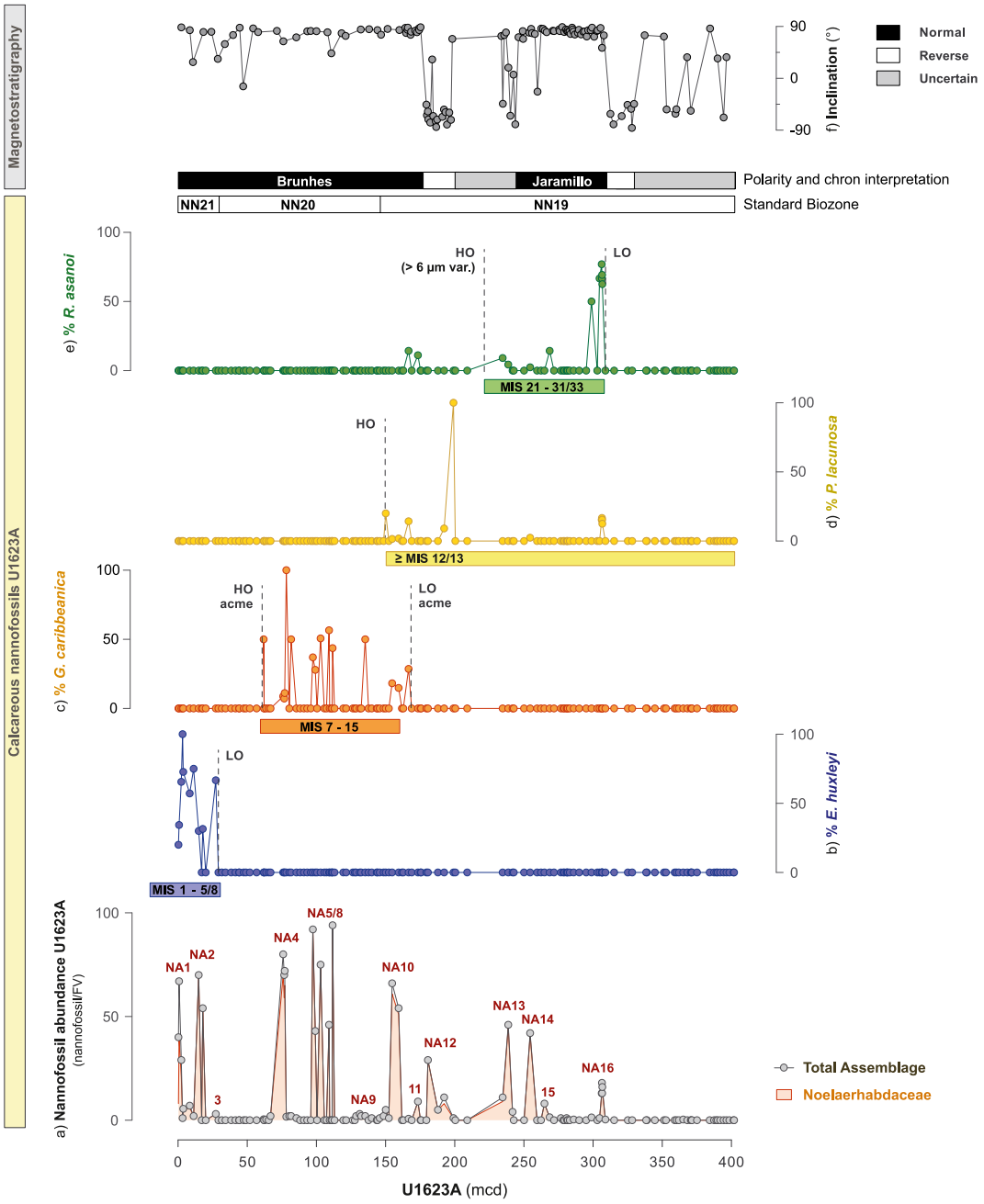

Fig. 3. Calcareous nannofossil content biostratigraphic scheme, magnetostratigraphic inclination data and polarity definition at Hole U1623A. **a)** Concentration of nannofossils in samples (per field of view; FV); Represenation of the total assemblage (grey line) and Noelaerhabdaceae specimens (filled with orange). Nannofossil abundance events (NA1 to 16) are labeled. Percent abundances (%) of biostratigraphic index species: **b)** % *Emiliania huxleyi*; **c)** % *Gephyrocapsa caribbeanica*; **d)** % *Pseudoemiliania lacunosa*; **e)** % *Reticulofenestra asanoi* > 6 µm; **f)** Paleomagnetic inclination after 30 mT peak AF demagnetization. LO = Lowest Occurrence; HO = Highest Occurrence. The lower bars indicate MIS (Marine Isotope Stages), according to Lisiecki and Raymo, 2005, and determined by the presence of the biostratigraphic index species. Summarized calcareous nannofossil biozonation (Martini 1971) and polarity interpretation and chron identification (Gradstein and Ogg, 2020) are included. A list of calcareous nannofossil biohorizons at Hole U1623A and their mbsf and mcd depths is includded in Supplementary Table S2. (For interpretation of the references to color in this figure legend, the reader is referred to the Web version of this article.)

Predicted inclinations for these sites for a geocentric axial dipole (GAD) are around 83°, which is nearly identical to the modern geomagnetic inclination of 81.6°. Accordingly, we base our magnetostratigraphic interpretation on inclination values alone.

A total of 35 of the 40 samples in Hole U1621A contain inclination values within 15° of expected values for normal polarity for a GAD, indicating that sediments recovered at Hole U1621A were either all or mostly deposited during the most recent normal Brunhes Chron (C1n; 0–773 ka; Fig. 2e). Two samples from the final core recovered in this hole, Core U1621A-26X, contained negative inclinations of −26° and −34.4°. While it is possible that these samples may reflect an interval of reverse polarity, they are values that are much shallower than would be expected for a GAD and are samples from a heavily disturbed XCB core. Thus, we leave these samples uninterpreted and provide a limiting constraint that sediments deposited above 19,293. mcd in Core U1621A-25X must be younger than 773 ka (Table 1).

Samples from Hole U1623A contain values that are consistent with GAD inclinations for both normal and reverse polarity. While samples in

Table 1
Magnetostratigraphic constraints. The constraint for C1r.1n (t) at Hole U1623A includes both possible interpretations described in the text. (o) = onset; (t) = termination.

Event	Top Depth (mbsf)	Bottom Depth (mbsf)	Midpoint (mbsf)	Top Depth (mcd)	Bottom Depth (mcd)	Midpoint (mcd)	Age (ka)
Hole U1621A							
C1n (o)	177.47	–	–	192.93	–	–	<773
Hole U1623A							
C1n (o)	163.59	169.33	166.46	175.29	179.49	177.39	773
C1r.1n (t)	185.49 (211.7)	214	199.75 (212.85)	197.25 (243.79)	246.09	221.67 (244.94)	990
C1r.1n (o)	271.16	274.91	273.04	307.78	312.53	310.16	1071

the upper 50 m seem noisy, we interpret the upper 175.29 mcd (Cores U1623A-1H to 28X) and between 246.09 and 307.78 mcd (Cores U1623A-34X to 41X) as intervals of normal polarity that correspond to the Brunhes Chron (C1n; 0–773 ka) and Jaramillo Subchron (C1r.1n; 990–1071 ka), respectively (Fig. 3f; Table 1). There is uncertainty in the depth of the upper Jaramillo reversal (C1r.1n(t); 990 ka), that results from an interval of uncertain polarity containing both positive and negative inclination values extending from 198.24 mcd in Core U1623A-30X to 243.79 mcd in Core U1623A-34X, notably surrounding an interval that was very challenging to drill with poor recovery between 199 and 232 mcd due to the presence of a very stiff coarse diamicton (Lucchi et al., 2026). Conservatively, we leave this interval as an interval of uncertain polarity (Fig. 3f); however, we strongly suspect the upper Jaramillo reversal is located near the base of this uncertain interval between 243.79 and 246.09 mcd in Core U1623A-34X (depths for both interpretations are included in Table 1). An interval of reverse polarity between 312.53 mcd in Core U1623A-42X and 329.64 mcd in Core U1623A-44X was likely deposited below the Jaramillo Subchron in C1r.2r (1071–1180 ka); however, no clear pattern can be determined below 337.27 mcd, and this is left uninterpreted (Fig. 3f). This is most likely the result of challenges in XCB drilling near the base of the hole, where sediments described as diamictons became more common (Lucchi et al., 2026).

4.4. XRF Ca/Ti and Sr/Ti elemental ratios at site U1623

The Ca/Ti and Sr/Ti XRF profiles at Site U1623 (i.e., presented here on logarithmic scale) show overall strong covariation, with no significant differences observed at the resolution analysed in this study (Fig. 4). Below 315 mcd, the Ca/Ti exhibits a more pronounced variability of high frequency, not entirely mirrored in the Sr/Ti profile. This interval is nearly barren of nannofossils (i.e., just one sample yielded a minimal nannofossil representation) and lacks NA (Figs. 3 and 4).

All defined NA events at Site U1623 align well with increases in both Ca/Ti and Sr/Ti profiles (Fig. 4). This correspondence supports the interpretation that increases in Ca and Sr reflect enhanced sedimentary $CaCO_3$ concentration. The correspondence with enhancemens in Sr further reinforces a linkage with pelagic $CaCO_3$ at Site U1623 (Fig. 4).

5. Discussion

Calcareous nannofossils originating from Noelaerhabdaceae, the dominant calcifying phytoplankton family in nannofossil assemblages at Sites U1621 and U1623 (Figs. 2 and 3), are small in size (i.e., typically ranging between ~2 and 7.5 μm; Bown, 1998; Young et al., 2003). Due to their small dimensions, these nannofossils are more susceptible to dissolution than larger-sized taxa (e.g., Gibbs et al., 2004). Poorly preserved Quaternary assemblages often show an underrepresentation of this group, likely reflecting a preservation bias. Sediments dominated by the small and dissolution-prone Noelaerhabdaceae specimens at the Bellsund Drift, suggest that dissolution had a limited impact on the overall structure and composition of nannofossil assemblages. IODP Sites U1621 and U1623 were cored at depths of 1,636 and 1,708 m below sea level, respectively, and under the dominant influence of Atlantic waters, which are supersaturated with respect to $CaCO_3$ (e.g., Huber et al., 2000). These depths correspond to modern calcite saturation states (Ω) ranging from 1.75 to 2 (Jutterström and Anderson, 2005), well above the chemical lysocline threshold of $\Omega \approx 0.8$ (Milliman et al., 1999). Together with the characteristics of the Noelaerhabdaceae dominated calcareous nannofossil assemblages in this study (Figs. 2 and 3), the location and seawater chemical conditions of the setting allow inference of favorable conditions for the preservation and representativeness of assemblage structure, when calcareous nannofossil specimens are recorded in the sedimentary successions.

5.1. Calcareous nannofossil biochronology of sites U1621 and U1623

The dominant representation of Noelaerhabdaceae taxa in the sediments from Sites U1621 and U1623 (Figs. 2 and 3) enables the identification of the main calcareous nannofossil biostratigraphic events of the mid-to-late Pleistocene and Holocene, as summarized by Gradstein and Ogg (2020). Integrated with the magnetostratigraphic scheme, calcareous nannofossil assemblages offer a biochronology for the sedimens retrieved at Holes U1621A and U1623A during IODP Expedition 403 (Figs. 2 and 3).

The LO of *E. huxleyi* is identified in Holes U1621A and U1623A at depths 74.80 and 28.23 mcd, respectively (Figs. 2 and 3). At Hole U1621A, the representation of this species is characterized by an innitially scarce occurrence, followed by a more continuous presence from 50.44 mcd toward the top of the section (Fig. 2). The first appearance datum (FAD) of this taxon is a well-documented biostratigraphic event, globally identified and calibrated to 280 ka in the Marine Isotope Stage (MIS) 8 (Raffi et al., 2006; Thierstein et al., 1977). This bioevent may be diachronous at high latitudes, possibly due to varying environmental conditions. Independent chemostratigraphic age model determination in the Norwegian and Greenland Seas suggests the FAD of *E. huxleyi* to have lagged in those latitudes until around 120 ka, during MIS 5 (e.g., Gard and Backman, 1990; Henrich and Baumann, 1994). Re-examining calcareous nannofossil biostratigraphy of the set of central Arctic cores, Razmjooei et al. (2023) recently proposed the interval above the FAD of *E. huxleyi* to be constrained at periods ranging from MIS 5. An intermediate age, ranging between MIS 8 and MIS 5, is here considered for the LO *E. huxleyi* at Holes U1621A and U1623A (Figs. 2 and 3; Table S2). At Hole U1621A, the scarce representation of *E. huxleyi* below 50.44 mcd (i.e., in one sample at ~73.9 mcd) may reflect an age older than MIS 5, whereas its more continuous presence above this depth suggests a younger age, ranging from MIS 5 (Fig. 2). The LO of *E. huxleyi* identifies the NN20/NN21 boundary of Martini (1971), defined at 74.8 mcd in Hole U1621A and at 28.23 mcd in Hole U1623A (Figs. 2 and 3; Table S2).

G. caribbeanica is present between 72.37 and 159.97 mcd in Hole U1621A and between 62.06 and 167.76 mcd in Hole U1623A (Figs. 2 and 3; Table S2). This interval equaotes the acme event of *G. caribbeanica* (Baumann et al., 2004; Bollmann et al., 1998), that spans from subpolar to equatorial latitudes across different oceanic basins (Flores et al., 2012; González-Lanchas et al., 2020, 2021a, 2021b, 2023; Rickaby et al., 2007; Saavedra-Pellitero et al., 2017). Timing of this acme is well-dated in Atlantic equatorial to subpolar environments (Bollmann et al., 1998; Flores et al., 2012; González-Lanchas et al., 2023) to central Arctic records (see Razmjooei et al., 2023 and

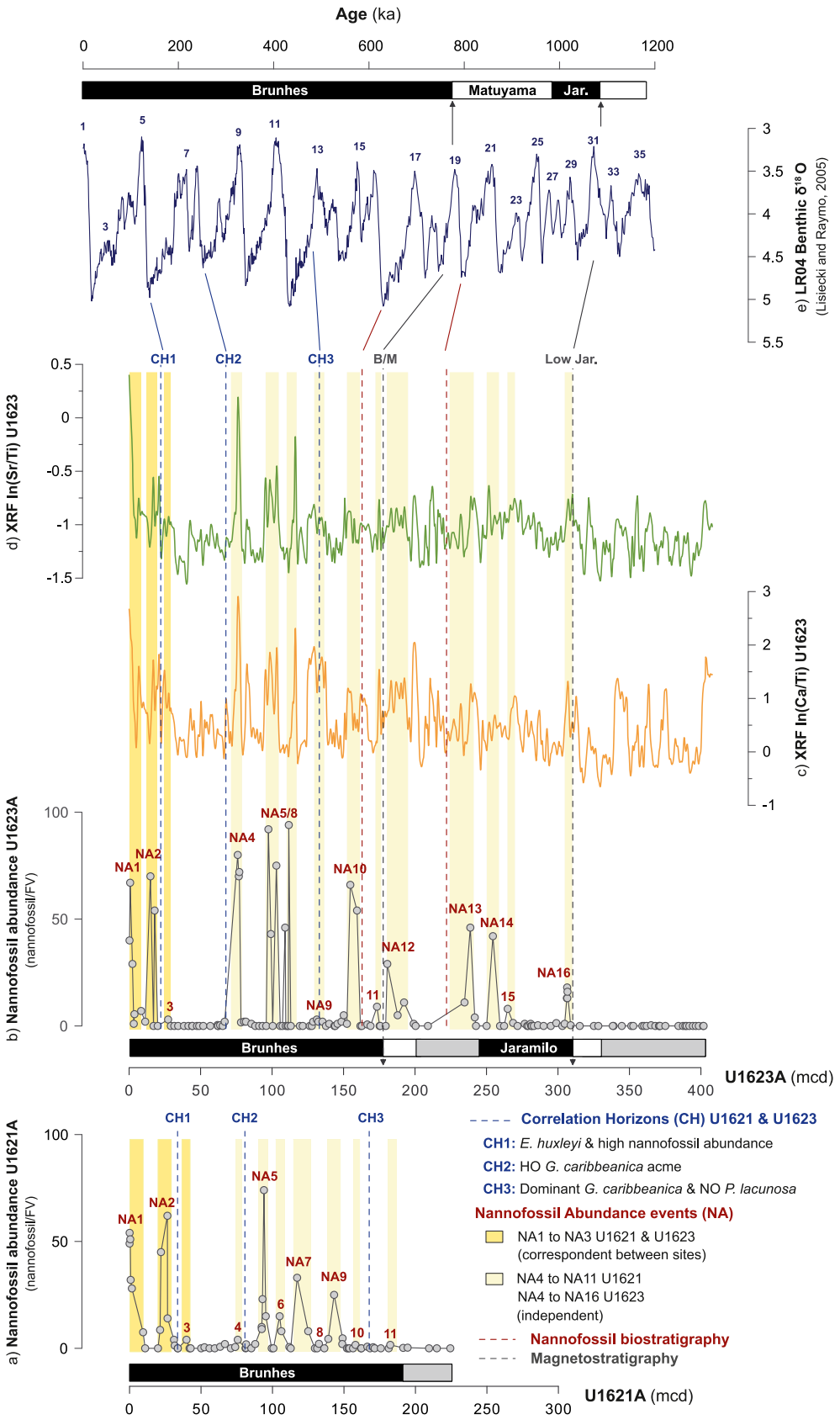

(caption on next page)

Fig. 4. Intercalibration of calcareous nannofossil biostratigraphy and magnetostratigraphy at Bellsund Drift Sites U1621 and U1623 integrated with sedimentary geochemical signatures, XRF-derived elemental ratios Ca/Ti and Sr/Ti, from Site U1623. Correlations between sites are established using Correlation Horizons (CH; shown in blue) defined in this study. The Bellsund Drift records are placed within the mid-to-late Pleistocene and Holocene glacial–interglacial (G/IG) framework over the past ~1 million years. **a)** Nannofossil concentrations at Hole U1621A, showing the identified Nannofossil Abundance (NA) events 1 to 11; **b)** Nannofossil concentrations at Hole U1623A, showing the identified NA events 1 to 16; **c)** XRF-derived Ca/Ti profile, expressed as ln(Ca/Ti); **d)** XRF-derived Sr/Ti profile, expressed as ln(Sr/Ti); **e)** Global LR04 benthic $\delta^{18}O$ stack from Lisiecki and Raymo (2005). NA events are plotted in red, with dashed yellow overlays indicating whether the event is site-specific (light yellow) or correlates between sites (dark yellow). Biostratigraphic and magnetostratigraphic boundaries used for correlation with the LR04 stack are indicated in red and black, respectively. (For interpretation of the references to color in this figure legend, the reader is referred to the Web version of this article.)

references therein), encompassing the mid-section of the Brunhes Chron (i.e., the so-called mid-Brunhes interval), with a maximum time span between ~250 and 600 ka (MIS 15 to MIS 7; e.g., Baumann and Freitag, 2004). The identification of this event (as LO and HO *G. caribbeanica* acme) at Holes U1621A and U1623A is considered to constrain the maximum age between MIS 15 and MIS 7 at the Bellsund Drift sites (Figs. 2 and 3).

The HO of *P. lacunosa* is recorded at 186.9 mcd in Hole U1621A and at 153.55 mcd in Hole U1623A (Figs. 2 and 3; Table S2). Available calibrations for this event in low-to mid-latitude records indicate an absolute age of 424 ka within glacial MIS 12 (Backman et al., 2012; Thierstein et al., 1977). Due to potential ecological limitations triggered by the extreme cold conditions of glacial MIS 12 at high latitudes, the HO of *P. lacunosa* is considered likely to have occurred during interglacial MIS 13 (Razmjooei et al., 2023). Considering those constraints, the HO *P lacunosa* could be placed between MIS 13 and 12 in the Bellsund Drift record (Figs. 2 and 3; Table S2). Because the HO of *P. lacunosa* in Hole U1621A is located close to the base of the drill hole, the evaluation of the continuity in the representation if this taxa at lower depths is hampered. As such, reworking affecting this boundary at Hole U1621A could not be completely discarded. The HO *P. lacunosa*, at 186.9 mcd at Hole U1621A and 153.55 mcd at Hole U1623A, defines the NN19/NN20 boundary by Martini (1971) in the Bellsund Drift Sites (Figs. 2 and 3; Table S2).

The species *R. asanoi* is found in the deeper Hole U1623A record, between depths 164.71 and 307.78 mcd (Fig. 3). According to the taxonomic definition for the biostratigraphic application of this taxa (e.g., Bown, 1998; Raffi, 2002; Wei, 1993), specimens with size >6 μm are considered as the criteria for the biostratigraphic determination of the LO and HO, placing those bioevents at 221.83 and 307.78 mcd in the Hole U1623A, respectively (Fig. 3 and Table S2). The common occurrence of *R. asanoi* >6 μm in sedimentary records from low-to mid--latitude environments constrains a mid-Pleistocene time frame between 1.1 and 0.9 Ma (Raffi et al., 2006), corresponding to MIS 33 to 23. Existing assessments for the high latitudes in the North Atlantic determined the first common occurrence of this group during MIS 31 (Marino et al., 2011) and the HO during peak interglacial MIS 21 (Sato et al., 2009). Integrating those determinations, the wider MIS 33/31 to 21 interval is here considered as the maximum age range to constrain the record of *R. asanoi* >6 μm (i.e., LO to HO) in the FS. This time span characterizes the interval between 221.83 and 307.78 mcd in Hole U1623A (Fig. 3; Table S2).

5.2. Drivers of production and sedimentary signatures at the Bellsund Drift

The southeastern FS is characterized by sediments relatively enriched in $CaCO_3$, compared to other areas in the region (Huber et al., 2000). Samples with presence of calcareous nannofossils at Sites U1621 and U1623, along with the regional depositional context at the Bellsund Drift, supports the in-situ origin and limited post-depositional alteration of those assemblages. Intervals of enhanced nannofossil abundance in the sedimentary record of Holes U1621A and U1623A are defined as NA events in this study (Figs. 2–4; Table S1). At Site U1623, the NA events appear tightly connected with intervals of elevated Ca and Sr signals in the XRF profiles. Increased biogenic $CaCO_3$ concentration, expressed in the sedimentary geochemical signatures during the NA events, suggests these XRF profiles reflect variations in pelagic production in the studied region (Fig. 4).

Nannofossil assemblages at Holes U1621A and U1623A are dominated by specimens belonging to the genus *Gephyrocapsa* of the Noelaerhabdaceae family. As a common feature to this genus, species are cosmopolitan, characterized by a broad ecological tolerance and the ability to thrive in a wide range of environmental conditions (e.g., Baumann and Freitag, 2004; Bollmann, 1997; Saavedra-Pellitero et al., 2017). These taxa optimize resource utilization, primarily light and nutrients, allowing them to rapidly grow in a range of environments. In records of modern to Quaternary age, their proliferation and bloom formation are commonly found in regions influenced by vertical nutrient supply from deep advection (e.g., upwelling zones; Andruleit et al., 2008; González-Lanchas et al., 2020; González-Lanchas et al., 2021a; Ziveri et al., 1995), as well as in regions receiving lateral nutrient input from riverine input (González-Lanchas et al., 2021b; Silva et al., 2008). The most common modern representative of this lineage, *E. huxleyi* , is a cosmopolitan species that dominates coccolithophore communities across several latitudes and environmental settings (see Tyrrell and Merico, 2004 and references therein). In the present-day FS, the seasonal warming induced by NAW influence during summer, combined with elevated irradiance, leads to favorable conditions for *E. huxleyi* blooms. These blooms have been observed to follow the northward extent of the NAW and to respond to its intensification (e.g., Oziel et al., 2020), reaching northern latitudes near the Arctic Front (Baumann et al., 2000; Dylmer et al., 2015; Samtleben and Schröder, 1992). Increased *E. huxleyi* abundance in Holocene sediments has been established as a proxy for seasonal NAW influence in the FS (see Matul et al., 2018 and references therein).

Enhanced calcifying phytoplankton production likely results from the combined effect of environmental drivers. These include non-limiting light availability and/or sufficient penetration, relatively warm temperatures and nutrient-enriched waters at the surface environment. Those drivers are considered to individually, or synergistically, stimulate the proliferation of communities at the southern FS. Importantly, seasonal to perennial sea-ice retreat and open-water conditions during warm phases are likely prerequisites for sustained calcifying phytoplankton production at the study area. The biogenic-geochemical covariance between NA events and Ca/Ti and Sr/Ti enhancements (Fig. 4) enables the identification of enhanced production, export and sedimentary concentration of $CaCO_3$, as primarily driven by calcifying phytoplanknton. Comparable intervals of enhanced nannofossil representation and sedimentary $CaCO_3$ concentrations have been observed in previous studies from the Nordic Seas and the FS (e.g., Baumann et al., 2000; Gard, 1986; Gard and Backman, 1990). Those are commonly interpreted as indicative of warmer periods related to interglacial phases. In line with the aforementioned studies, the influence of NAW and the northward displacement of the AF during interglacial stages is here considered as major paleoceanographic driver on the environmental conditions stimulating calcifying phytoplankton production at the FS. NAW influence operates through a dual mechanism: promoting surface warming and enhancing nutrient availability—via horizontal inputs, associated with NAW flux, and vertical advection, linked to AF dynamics. Conversely, barren intervals in the records are associated with conditions during glacial stages, characterized by

reduced NAW influence and a southward shift of the AF, suppressing nutrient supply, promoting overall surface cooling, and fostering variable, but persistent, sea-ice development at FS latitudes.

5.3. Orbitally-driven climate variability at the Bellsund Drift

Constrained by the chronostratigraphic framework established from the intercalibration of biostratigraphy and paleomagnetism, the NA events at Sites U1621 and U1623 are interpreted to correspond to interglacial conditions spanning the mid-to-late Pleistocene and Holocene (Fig. 4). This scheme provides an initial evidence of the structure of major Pleistocene climate transitions at the Bellsund Drift.

The NA1, recorded at both Sites U1621 and U1623, is associated with the Holocene. This interpretation is supported by the presence of *E. huxleyi* in nannofossil assemblages and by elevated pelagic production, as evidenced by the magnitude of NA1 and the increases in Ca/Ti and Sr/Ti ratios (Figs. 2–4). Simmilarly constrained by *E. huxleyi* and elevated pelagic production, NA2 is a prominent feature at both Sites U1621 and U1623, and extends across a relatively prolongued depth interval in both records (Figs. 2–4). Elevated Ca/Ti and Sr/Ti ratios indicate enhanced pelagic production, which, together with the micropaleontological evidence, supports its correspondence with interglacial MIS 5 conditions. At Site U1623, the NA2 displays a double-peaked structure, highlighting the prolonged nature of the event and, possibly, recording conditions differentiable to the sub stages of interglacial MIS 5 (i.e., MIS 5e and MIS 5a) in the Bellsund Drift sediments. Similar micropaleontological and sedimentary characteristics—increased $CaCO_3$ content—have been documented for this interval in previous studies (e.g., Gard, 1986, 1988; Henrich and Baumann, 1994), adding support to this interpretation. Building on these findings, the persistent and, plausibly, intensified influence of NAW during the MIS 5 period may have contributed to elevated pelagic production and biogenic $CaCO_3$ concentration (Fig. 4). At Site U1623, the NA2 event also shows continuity with NA1—nannofossil abundances do not entirely decrease between them, but instead remain modestly represented (Figs. 3 and 4). This structure is also expressed in the XRF profiles, likely reflecting a succession encompassing evidence of MIS 3, between NA2 and NA1 (Fig. 4). This stratigraphic interpretation may suggests that conditions during glacial MIS 4 were relatively mild, or insufficient to completely suppress calcifying phytoplankton proliferation and production at the southestern FS. We tentatively suggest that more prolonged seasonal NAW inflow during this glacial period may have affected the FS. Detailed analysis at a higher resolution will be required for a full discrimination of hiatuses affecting that part of the record and to confirm the propossed hypothesis. Based on the LO *E. huxleyi* and the similar structure of the NA1 and NA2 events, with representation of this species across both sites, we define the Correlation Horizon 1 (CH1) between Site U1621 (32.64 mcd) and Site U1623 (18.92 mcd; Fig. 4; Table S1). This horizon marks the lower boundary of the interval that comprises the Holocene to MIS 5 section at both the U1621 and U1623 sites at the Bellsund Drift (Fig. 4).

Below CH1, both records are marked by an interval with very sparse nannofossil content, extending down to the HO of *G. caribbeanica* acme—located at 72.37 mcd in Hole U1621A and 62.06 mcd in Hole U1623A (Figs. 2–4; Table S2). Within this interval, the NA3 event is modestly expressed in both records and is primarily composed of *E. huxleyi* specimens (Figs. 2–4). At Site U1621, a second low-amplitude event, termed NA4, is also identified; this is characterized by trace amounts of *G. caribbeanica* (Fig. 2). In contrast, the lowermost part of this interval at Site U1623 is completely barren of calcareous nannofossils (Fig. 3). The geochemical composition of sediments at Site U1623 is marked by relatively low Ca and Sr concentrations, within a "flat-shaped" profile of reduced variability, in comparison with the rest of the record—particularly evident in the Sr/Ti ratio (Fig. 4). Within the broader context of nannofossil scarcity, the near-exclusive presence of *E. huxleyi* and the absence, or only minor occurrence, of *G. caribbeanica* (Fig. 2), support the correlation of this interval with MIS 6 to 8 in both sites (Fig. 4). This chronostratigraphic-based interpretation is strongly reinforced by analogous micropaleontological and sedimentary conditions documented in the Nordic Seas, where the MIS 6 to 8 interval is similarly characterized by nannofossil scarcity and reduced $CaCO_3$ concentrations in sediments (e.g., Henrich and Baumann, 1994). The striking similarity across geographically separated but paleoceanogrpahically connected records provides robust and independent validation of the proposed correlation and offers critical insights into climate dynamics that prevailed during the MIS 6 to 8 interval. As such, interglacial MIS 7 appears to be "muted" in the Bellsund Drift records. We explore whether biotic, environmental, or depositional controls (or their convergence) may explain this uncertain, or subdued, expression.

First, evolutionary or adaptive constraints may have influenced calcifying phytoplankton proliferation and production in high-latitude settings, shaping the sedimentary signature of this interval at the Bellsund Drift. Interglacial MIS 7 represents a transitional phase in global dominance between the phylogenetically related *G. caribbeanica* and *E. huxleyi* (e.g., Beaufort et al., 2022; Bendif et al., 2019). These species are key contributors to pelagic production and sedimentary $CaCO_3$ stock in mid-to late Pleistocene sedimentary records (e.g., Baumann and Freitag, 2004; Beaufort et al., 2022; Jin et al., 2022; Rickaby et al., 2007). While *E. huxleyi* is thought to begin its dominance at low latitudes, as early as MIS 8, records in northern high latitudes and the central Arctic Ocean suggest the onset of this taxon closer to MIS 5 (see Razmjooei et al., 2023 and references therein). A more prolonged, or regionally delayed, evolutionary shift between these two globally dominant taxa in the northern high-latitude settings may had resulted in "non-consolidated" calcifying phytoplankton communities (i.e., a population overally reduced in number due to evolutionary/adaptive constraints). This configuration could have been key in driving the "muted" biogenic $CaCO_3$ signal in the Bellsund Drift sediments during MIS 7, despite presumed prevailing warm conditions across that interglacial stage. Second, anomalous climatic conditions during MIS 7 cannot be ruled out as a fundamental factor limiting calcifying phytoplankton proliferation and, possibly, influencing the aforementioned phylogenetic transition in northern high-latitude environments. The parallels with records in the Nordic Seas (Henrich and Baumann, 1994), may suggest large-scale changes in the northward advection of warm NAW during this interval, possibly involving variations in intensity, frequency, and/or pathway. More extensive sea-ice cover in the southwestern FS (i.e., seasonal or spatial) may have played a role in restricting calcifying phytoplankton. Alternatively, a similar ecological signal may have resulted from enhanced melting, indicating intensified warming. Melting and freshwater input from Svalbard could have intensified surface stratification and turbidity, hampering nutrient advection and light penetration, ultimately reducing calcifying phytoplankton production, as reported in the area during Termination I (Colmenero-Hidalgo et al., 2009; Lucchi et al., 2013). Thirdly, the elevated thickness of the sedimentary succession containing the MIS 6 to 8 interval is highly comparable between Sites (~48 m at Hole U1621A and ~40 m at Hole U1623A; Figs. 2–4), within a relatively brief interval of ~170 kyr duration (Fig. 4). This suggests that additional regional sedimentary processes may have influenced the sedimentary characteristics of this interval in both sites. Consistent with the hypothesized enhanced melting activity during MIS 7, intensified discharges from the Svalbard margin, enhancing terrigenous inputs, are supported by relatively elevated Ti concentrations in the geochemical profiles of Site U1623 (i.e., low Sr/Ti and Ca/Ti; Fig. 4), and may account for both the subdued calcifying phytoplankton production and the unusually thick sedimentary sequence observed at both sites. Targeted multi-proxy studies, accounting for the reconstruction of local conditions at a higher resolution, will be essential to unravel the complexity of this interval at the FS.

The interval dominated by *G. caribbeanica* at the Bellsund Drift records extends from 72.37 to 159.97 mcd at Hole U1621A and from 62.06

to 167.76 mcd at Hole U1623A (Figs. 2–4; Table S2). The upper boundary of this interval, marked by the HO of *G. caribbeanica*, defines Correlation Horizon 2 (CH2) between Sites U1621 and U1623 (Fig. 4; Table S1). Because *E. huxleyi* is absent at NA events in Holes U1621A and U1623A below CH2, that part of the records likely has its upper boundary at MIS 9, with progressively older intervals below. The Correlation Horizon 3 (CH3) between sites is defined above the HO of *P. lacunosa*, coexistent with a maintained dominance of *G. caribbeanica* in records. This corresponds to the MIS 12/13 boundary (Fig. 4; Table S2). Below the CH3, the longer U1623 succession records the coexistence of the species *G. caribbeanica* and *P. lacunosa.* This interval frames a chronology that extends back to the MIS 15, determined by the LO *G. caribbeanica* acme at Site U1623 (Fig. 4; Table S2).

At the two Bellsund sites, the mid-Brunhes interval coincides with a sequence of NA events of highest magnitude, NA5 to NA9 at Site U1621 and NA4 to NA10 at Site U1623 (Figs. 2–4). At Site U1623, the structure of those NA events shows a clear correspondence with peaks in the geochemical ratios, particularly notable in comparison with the Sr/Ti profile (Fig. 4). The prominent peak abundances of calcareous nannofossils, dominated by *G. caribbeanica*, together with the elevated Sr and Ca ratios in XRF profiles, are consistent with previous peak enhancements in sedimentary $CaCO_3$ concentrations characterizing the mid-Brunhes interval (i.e., MIS 9 to 15) in the Norwegian Sea and FS (Gard, 1988; Henrich and Baumann, 1994). While those earlier studies support our interpretation, the pattern identified at the Bellsund Drift stands out for its clarity and internal consistency, offering a robust and independently constrained view of enhanced production and sedimentary concentration of biogenic $CaCO_3$ during this interval. Consistent with integrated records, a large-scale intensification of the northward advection of the warmer NAW is inferred to have promoted favorable conditions for calcifying phytoplankton proliferation and production during interglacial phases MIS 9, 11, 13, and 15 (Fig. 4).

The characteristics of the mid-Brunhes interval at the Bellsund Drift show, as well, a strong agreement with globally distributed records. The *G. caribbeanica* acme is characterized by a notable increase in the rates of coccolithophore growth and calcification at physiological level (González-Lanchas et al., 2023; Rickaby et al., 2007), that is consistently reflected as increases in the sedimentary $CaCO_3$ stock globally (Baumann and Freitag, 2004; Rickaby et al., 2007; Beaufort et al., 2022; Bollmann et al., 1998; Flores et al., 2012; González-Lanchas et al., 2020, 2021a, 2023; Jin et al., 2022; Saavedra-Pellitero et al., 2017). The typically enhanced biogenic $CaCO_3$ sedimentary stock associated with this calcifying phytoplankton acme is here inferred from the magnitude of NA events and further supported by correspondence with the relatively enhanced Sr and Ca concentrations (Fig. 4). Coccolith calcite appears to be significantly enriched in Sr during the *G. caribbeanica* acme across records from different latitudes (e.g., Rickaby et al., 2007). Intensified $CaCO_3$ export, driven by the enhanced proliferation and production of these specimens, could be considered a key factor behind the enhanced sedimentary Sr/Ti ratios across the mid-Brunhes (Fig. 4). Extrapolating the conditions of enhanced coccolithophore growth, calcification and $CaCO_3$ production to the high-latitude FS setting reinforces the necessary role of a globally distributed paleoceanographic driver of this calcifying phytoplankton event, plausibily involving seawater chemical changes of translatitudinal extent (González-Lanchas et al., 2023; Rickaby et al., 2007).

The NA5 at Site U1621 and NA5 to NA8 at Site U1623 emerge as high-magnitude features within the mid-Brunhes interval at the Bellsund Drift sites (Fig. 4). Interglacial MIS 11, often considered the apex of the mid-Brunhes, is characterized by peak *G. caribbeanica* representation and elevated sedimentary $CaCO_3$ content across widespread oceanographic settings (e.g., Baumann and Freitag, 2004; Flores et al., 2012; González-Lanchas et al., 2020, 2021a,González-Lanchas et al., 2025 2023; Rickaby et al., 2007; Saavedra-Pellitero et al., 2017), including the adjacent Norwegian Seas (Henrich and Baumann, 1994). Based on strong similarities with this well-documented interglacial, we associate NA5 at Site U1621 and NA5 to NA8 at Site U1623 with MIS 11 features. At Site U1623, the lowermost NA9 and NA10 events correspond to MIS 13 and MIS 15, based on the coexistence of *G. caribbeanica* and *P. lacunosa* (Figs. 3 and 4; Table S2). This integrated view provides a well-constrained identification of the complete mid-Brunhes interval in the FS region for the first time. Given the importance of this period for understanding global climate (e.g., Barth et al., 2018; Yin and Berger, 2010) and marine carbon cycle dynamics (e.g., Barker et al., 2006; González-Lanchas et al., 2023), the Bellsund Drift emerges as a valuable high-latitude sedimentary end-member for future research.

Below CH3 at Site U1623, the absence of *G. caribbeanica* across NA11 and NA12, along with the presence of *P. lacunosa* and small-sized *R. asanoi* specimens ($\leq$6 μm), suggests that these events represent interglacials predating MIS 15 and postdating MIS 21 (Figs. 3 and 4). This interval likely encompasses MIS 17 and MIS 19, with NA11 and NA12 correlated to these stages, respectively (Fig. 4). This correlation is supported by similarities in nannofossil assemblage structures with Norwegian Sea records (Henrich and Baumann, 1994). Notably, NA12 also aligns stratigraphically with the Matuyama-Brunhes geomagnetic reversal at Site U1623 (Fig. 3), which has been globally dated to the late MIS 19 (Channell et al., 2020; Shackleton and Opdyke, 1973). Both NA11 and NA12 are more subdued than the younger and more prominent NA events at the upper part of the record, a pattern also reflected in the geochemical Ca/Ti and Sr/Ti profiles, which only show moderate relative increases in Ca and Sr (Fig. 4). Slightly lower sampling resolution between ~210 and 240 mcd limits direct correlation between nannofossil abundance and geochemical signals in that part of the Site U1623 succession. The subsequent NA12 to NA16 interval, marked by the presence of *R. asanoi* specimens >6 μm (Fig. 3), is assigned to MIS 21 through MIS 31 (Fig. 4). NA events within this interval correspond to relative enhancements in the Ca/Ti and Sr/Ti ratios, although of generally lower amplitude compared to the overlying mid-Brunhes to Holocene section. We interpret NA16 as correlating with the lower boundary of the Jaramillo Subchron, providing a key chronological anchor that supports the correspondence of NA16 to interglacial MIS 31 (Fig. 4). No NA events are recorded below this boundary at the resolution of this study. Some variability in sedimentary Ca content is nevertheless observed, although the signal is less pronounced in Sr (Fig. 4). Given that Sr is more directly associated with biogenic $CaCO_3$ production, our integrated data suggest limited calcifying phytoplankton proliferation and pelagic production by this group prior to this boundary (i.e., MIS 31, ~1.1 Ma).

In summary, the NA events identified at Sites U1621 and U1623, when integrated with the geochemical Ca/Ti and Sr/Ti ratios, reflect episodes of enhanced surface pelagic production. Their alignment with similar nannofossil assemblages and sedimentary signatures in records from the Norwegian Seas and the FS in previous research points to large-scale oceanographic forcing, namely the NAW advection across this Arctic gateway. The recurrence and structure of these events suggest orbitally forced G/IG variability, with regional interglacial warming and intensified NAW inflow likely promoting the proliferation and production of calcifying phytoplankton during interglacials, imprinting the Bellsund Drift sediments by enhanced $CaCO_3$ concentrations. A reduction in the frequency of NA events, accompanied by increased amplitude of the abundance peaks, is observed at 177.39 mcd at Site U1623, with a clear correspondence in the geochemical Ca and Sr profiles (Fig. 4). This upper portion of the U1623 sequence aligns stratigraphically with the entire U1621 record. Integrated biostratigraphic and magnetostratigraphic data indicate it spans the last ~773 kyr, corresponding to the Brunhes chron (Fig. 4). The shift in micropaleontological and sedimentary geochemical patterns reflects changes in the frequency and amplitude of G/IG variability, likely associated with the Mid-Pleistocene Transition (MPT). Given the inferred link between NA events and calcifying phytoplankton ecology, the transition may signal a fundamental reorganization in the recurrence and intensity of NAW through the FS. In the upper ~120 mcd at Site U1623, NA events become

significantly amplified and coincide with more marked increases in Ca and, specially, Sr in the XRF profiles, a pattern also observed in the NA record at Site U1621 (Fig. 4). This structure and geochemical characteristics is interpreted as an expression of the increase in amplitude of G/IG cyclicity characterizing the mid-Brunhes transition in the FS. The enhanced calcifying phytoplankton production, recorded in both assemblage composition and sedimentary geochemical ratios, suggests improved ecological conditions for the proliferation and production of this group. These conditions, linked to intensified NAW-driven regional warming, reduced sea-ice, shifts in nutrient regimes, and altered competition between phytoplankton groups, may reflect the onset of Arctic amplification processes after the mid-Brunhes event (~400 ka). The timing of this feature is consistent with previous evidence from the central Arctic (e.g., Cronin et al., 2017). Accordingly, we propose that the Bellsund Drift records could offer valuable insight for the analysis of the evolution of warming and Arctic amplification mechanisms from the Pleistocene.

6. Conclusions

This study establishes a first well-constrained chronostratigraphic framework for the Bellsund Drift sediments in the southeastern Fram Strait (FS), based on the intercalibration between calcareous nannofossil and magnetostratigraphic records from Sites U1621 and U1623. Integrated with X-ray Fluorescence (XRF)-derived geochemical elemental ratios at Site U1623, the records document a robust signal of pelagic $CaCO_3$ production across the past ~1 million years. Distinct increases in nannofossil abundances, defined here as Nannofossil Abundance (NA) events, closely correspond with peak enhancements in Ca/Ti and Sr/Ti ratios, indicating orbitally paced fluctuations in sedimentary $CaCO_3$ concentration, likely driven by calcifying phytoplankton production. These patterns are interpreted as reflecting NAW-driven changes in surface ecologies modulated by glacial–interglacial (G/IG) climate variability. The stratigraphic structure and taxa composition of NA events reflect similar signals from lower-latitude records, allowing the identification of interglacial Marine Isotope Stages (MIS) 31, 19, 15–9, 5, and the Holocene, and the characterization of the Mid-Pleistocene Transition (MPT) and the Mid-Brunhes Event (MBE) at the FS. In addition to its stratigraphic value, the presence of Noelaerhabdaceae taxa across the studied interval, including both the modern cosmopolitan *Emiliania huxleyi* and its Pleistocene precursors, highlights the Bellsund Drift as a high-latitude archive for exploring the long-term evolutionary and ecological dynamics of calcifying phytoplankton and $CaCO_3$ production. Altogether, this study highlights the Bellsund Drift sediments as an exceptional record of orbitally forced paleoceanographic and paleoclimatic variability across the last past ~1 million years.

Author contribution

The study was designed by AGL and BR. Nannofossil sample selection and preparation were conducted by AGL and MAB. Magnetostratigraphic sample analysis and data integration were conducted by BR and YZ. Spliced depth scale was developed by JG and YR. Formal analysis, calculation, data integration, and interpretations were conducted by AGL and BR. REMR provided resources. AKIUK, LRM, BR, TAR, KSJ, LSJ, and JY conducted the XRF measurements of Site U1623 in College Station (Texas, USA). Manuscript visualization and writing were led by AGL with contributions and feedback from all the coauthors, BR, MAB, SDS, ACG, JG, KH, YR, YS, YZ, REMR, AKIUK, LRM, YJ, RGL, KSJ, TAR, LD, GG, NG, LH, MI, ARL, OLR, YL, YS and AVS.

Declaration of competing interest

The authors declare that they have no known competing financial interests or personal relationships that could have appeared to influence the work reported in this paper.

Acknowledgements

The participation of AGL at IODP Expedition 403 and the development of this research is funded by the UK-IODP Moratorium Award funded by NERC (Natural Environmental Research Council) ref. NE/Z000300/1 (Co-evolution of phytoplankton and environment at the Fram Strait). Additional support from the NERC-funded PUCCA project (Photosynthetic Underpinnings of Coccolithophore Calcification) NE/V011049/1 is acknowledged. BR, YR, IK, LRM, KSJ, GG, NG, LH, AL, and OLR received support from the US Science Support Program (US National Science Foundation Division of Ocean Sciences (NSF-OCE) Award 1450528. Participation of RGL was funded through MUR for ECORD-IODP Italia. MAB acknowledges the project PID2021-126495NB-C33 funded by the Spanish Ministry of Science, Innovation, and Universities. SDS acknowledges funding from the European Union, ERC Consolidator Grant AGENSI (818449) and ERC Synergy Grant i2B (101118519). ACG and JG thank the German IODP office for travel support. Exp 403 and the JRSO were funded by NSF-OCE award 1326927. Sediment materials for this study were provided by IODP. The *JOIDES Resolution* provided analytical infrastructure and facilities for this research. Scientific technicians, drilling operators, and crew are acknowledged for their labour and support. The authors thank Larry A. St. John for his contribution to Site U1623 XRF scanning. Dr. Karl-Heinz Baumann is acknowledged for the insightful discussions about nannofossil taxonomy and calcifying phytoplankton ecologies at the Fram Strait. Juan Pablo Perez Panera and Denise Kulhanek are acknowledged for their detailed revisions that greatly benefitted the presentation of this manuscript.

Appendix A. Supplementary data

Supplementary data to this article can be found online at https://doi.org/10.1016/j.quascirev.2026.109838.

Data availability

All original data produced for this work is archived and publically accesible at the Zenodo and Magnetics Information Consortium (MagIC) repositories as:González-Lanchas, A., Reilly, B.T. , Bárcena, M.A., De Schepper, S., Gebhardt, C., Gruetzner, J., Husum, K., Rosenthal, Y., Suganuma, Y., Zhong, Y., Rickaby, R.E.M., Kapuge, A.K.I.U., Monito, L. R., Yeon, J., Lucchi, R.G., St. John, K., Ronge, T.A., Duxbury, L., Goss, G., Greco, N., Haygood, L., Iizuka, M., Lam, A.R., Libman-Roshal, O., Liu, Y., Sakai, Y. and Sijinkumar A.V (2025). Calcareous nannofossil, paleomagnetic, and X-ray fluorescence data in support of González-Lanchas et al., "A paleoclimate reference record spanning the last 1 million years from the Fram Strait (Sites U1621 and U1623, IODP Expedition 403)" [Data set]. Zenodo. https://doi.org/10.5281/zenodo.17244889González-Lanchas, A., Reilly, B.T. , Bárcena, M.A., De Schepper, S., Gebhardt, C., Gruetzner, J., Husum, K., Rosenthal, Y., Suganuma, Y., Zhong, Y., Rickaby, R.E.M., Kapuge, A.K.I.U., Monito, L.R., Yeon, J., Lucchi, R.G., St. John, K., Ronge, T.A., Duxbury, L., Goss, G., Greco, N., Haygood, L., Iizuka, M., Lam, A.R., Libman-Roshal, O., Liu, Y., Sakai, Y. and Sijinkumar A.V (2026). "A paleoclimate reference record spanning the last 1 million years from the Fram Strait (Sites U1621 and U1623, IODP Expedition 403)" [Data set]. Magnetics Information Consortium (MagIC). https://doi.org/10.7288/V4/MAGIC/20255

References

Alexanderson, H., Backman, J., Cronin, T.M., Funder, S., Ingólfsson, Ó., Jakobsson, M., Landvik, J.Y., Löwemark, L., Mangerud, J., März, C., 2014. An arctic perspective on dating mid-late Pleistocene environmental history. Quat. Sci. Rev. 92, 9–31.

Andruleit, H., Lückge, A., Wiedicke, M., Stäger, S., 2008. Late Quaternary development of the Java upwelling system (eastern Indian Ocean) as revealed by coccolithophores. Mar. Micropaleontol. 69, 3–15.

Backman, J., Jakobsson, M., Løvlie, R., Polyak, L., Febo, L.A., 2004. Is the central Arctic Ocean a sediment starved basin? Quat. Sci. Rev. 23, 1435–1454.
Backman, J., Raffi, I., Rio, D., Fornaciari, E., Pälike, H., 2012. Biozonation and biochronology of Miocene through Pleistocene calcareous nannofossils from low and middle latitudes. Newsl. Stratigr. 45, 221–244.
Barker, S., Archer, D., Booth, L., Elderfield, H., Henderiks, J., Rickaby, R.E., 2006. Globally increased pelagic carbonate production during the mid-Brunhes dissolution interval and the CO2 paradox of MIS 11. Quat. Sci. Rev. 25 (23–24), 3278–3293.
Barth, A.M., Clark, P.U., Bill, N.S., He, F., Pisias, N.G., 2018. Climate evolution across the Mid-Brunhes transition. Clim. Past 14, 2071–2087.
Baumann, K.-H., Andruleit, H., Samtleben, C., 2000. Coccolithophores in the Nordic Seas: comparison of living communities with surface sediment assemblages. Deep Sea Res. Part II Top. Stud. Oceanogr. 47, 1743–1772.
Baumann, K.-H., Böckel, B., Frenz, M., 2004. Coccolith contribution to South Atlantic carbonate sedimentation. Coccolithophores: from Molecular Processes to Global Impact. Springer, pp. 367–402.
Baumann, K.-H., Freitag, T., 2004. Pleistocene fluctuations in the northern Benguela current system as revealed by coccolith assemblages. Mar. Micropaleontol. 52, 195–215.
Beaufort, L., Bolton, C.T., Sarr, A.-C., Suchéras-Marx, B., Rosenthal, Y., Donnadieu, Y., Barbarin, N., Bova, S., Cornuault, P., Gally, Y., 2022. Cyclic evolution of phytoplankton forced by changes in tropical seasonality. Nature 601, 79–84.
Bendif, E.M., Nevado, B., Wong, E.L., Hagino, K., Probert, I., Young, J.R., Rickaby, R.E., Filatov, D.A., 2019. Repeated species radiations in the recent evolution of the key marine phytoplankton lineage gephyrocapsa. Nat. Commun. 10, 4234.
Bendif, E.M., Probert, I., Archontikis, O.A., Young, J.R., Beaufort, L., Rickaby, R.E., Filatov, D., 2023. Rapid diversification underlying the global dominance of a cosmopolitan phytoplankton. ISME J. 17, 630–640.
Blindheim, J., Osterhus, S., 2005. The nordic seas, main oceanographic features. Geophys. Monogr.-Am. Geophys. Union 158, 11.
Bollmann, J., 1997. Morphology and biogeography of gephyrocapsa coccoliths in Holocene sediments. Mar. Micropaleontol. 29, 319–350.
Bollmann, J., Baumann, K.H., Thierstein, H.R., 1998. Global dominance of gephyrocapsa coccoliths in the late Pleistocene: selective dissolution, evolution, or global environmental change? Paleoceanography 13, 517–529.
Bown, P.R., 1998. Calcareous Nannofossil Biostratigraphy. Springer.
Caricchi, C., Lucchi, R.G., Sagnotti, L., Macrì, P., Di Roberto, A., Del Carlo, P., Husum, K., Laberg, J.S., Morigi, C., 2019. A high-resolution geomagnetic relative paleointensity record from the Arctic Ocean deep-water gateway deposits during the last 60 kyr. G-cubed 20, 2355–2377.
Channell, J.E., Singer, B.S., Jicha, B.R., 2020. Timing of Quaternary geomagnetic reversals and excursions in volcanic and sedimentary archives. Quat. Sci. Rev. 228, 106114.
Colmenero-Hidalgo, E., Rigual Hernández, A., Lucchi, R., Bárcena, M., Sierro, F., Ja, F., de Vernal, A., Camerlenghi, A., 2009. Analysis of a new micropalaeontological record from the southern margin of the Svalbard archipelago (Arctic Ocean): preliminary results and palaeoceanographic implications. Geogaceta 46, 91–94.
Cronin, T.M., Dwyer, G.S., Caverly, E., Farmer, J., DeNinno, L.H., Rodriguez-Lazaro, J., Gemery, L., 2017. Enhanced arctic amplification began at the mid-Brunhes event~ 400,000 years ago. Sci. Rep. 7, 14475.
Dylmer, C., Giraudeau, J., Hanquiez, V., Husum, K., 2015. The coccolithophores Emiliania huxleyi and coccolithus pelagicus: extant populations from the Norwegian–Iceland seas and Fram Strait. Deep Sea Res. Oceanogr. Res. Pap. 98, 1–9.
Flores, J.-A., Filippelli, G.M., Sierro, F.J., Latimer, J., 2012. The "White Ocean" hypothesis: a late Pleistocene Southern Ocean governed by coccolithophores and driven by phosphorus. Front. Microbiol. 3, 233.
Forest, A., Wassmann, P., Slagstad, D., Bauerfeind, E., Nöthig, E.-M., Klages, M., 2010. Relationships between primary production and vertical particle export at the Atlantic-Arctic boundary (Fram Strait, HAUSGARTEN). Polar Biol. 33, 1733–1746.
Gard, G., 1986. Calcareous nannofossil biostratigraphy of late Quaternary Arctic sediments. Boreas 15, 217–229.
Gard, G., 1988. Late Quaternary calcareous nannofossil biozonation, chronology and palaeo-oceanography in areas north of the Faeroe-Iceland Ridge. Quaternary Science Reviews 7 (1), 65–78.
Gard, G., Backman, J., 1990. Synthesis of Arctic and Sub-Arctic coccolith biochronology and history of North Atlantic drift water influx during the last 500.000 years. Geological History of the Polar Oceans: Arctic Versus Antarctic, pp. 417–436.
GEBCO Bathymetric Compilation Group 2023, 2023. The GEBCO_2023 Grid - a Continuous Terrain Model of the Global Oceans and Land. NERC EDS British Oceanographic Data Centre NOC. https://doi.org/10.5285/f98b053b-0cbc-6c23-e053-6c86abc0af7b.
Gibbs, S.J., Shackleton, N.J., Young, J.R., 2004. Identification of dissolution patterns in nannofossil assemblages: a high-resolution comparison of synchronous records from Ceara Rise, ODP Leg 154. Paleoceanography 19.
González-Lanchas, A., Dorador, J., Flores, J.A., Rodríguez-Tovar, F.J., 2025. Surface-to-deep-ocean ecosystem responses to orbital-to-millennial-scale paleoceanographic variability across the mid-Brunhes at the Iberian margin. Global and Planetary Change 105205.
González-Lanchas, A., Flores, J.-A., Sierro, F.J., Bárcena, M.Á., Rigual-Hernández, A.S., Oliveira, D., Azibeiro, L.A., Marino, M., Maiorano, P., Cortina, A., 2020. A new perspective of the Alboran Upwelling system reconstruction during the Marine Isotope stage 11: a high-resolution coccolithophore record. Quat. Sci. Rev. 245, 106520.
González-Lanchas, A., Flores, J.A., Sierro, F., Sánchez Goñi, M., Rodrigues, T., Ausín, B., Oliveira, D., Naughton, F., Marino, M., Maiorano, P., 2021a. Control mechanisms of primary productivity revealed by calcareous nannoplankton from marine isotope stages 12 to 9 at the shackleton site (IODP site U1385). Paleoceanogr. Paleoclimatol. 36 e2021PA004246.
González-Lanchas, A., Hernández-Almeida, I., Flores, J.A., Sierro, F.J., Guitian, J., Stoll, H.M., 2021b. Carbon isotopic fractionation of alkenones and gephyrocapsa coccoliths over the late Quaternary (Marine isotope stages 12–9) glacial-interglacial cycles at the Western tropical Atlantic. Paleoceanogr. Paleoclimatol. 36 e2020PA004175.
González-Lanchas, A., Rickaby, R.E.M., Sierro, F.J., Rigual-Hernández, A.S., Alonso-García, M., Flores, J.A., 2023. Globally enhanced calcification across the coccolithophore Gephyrocapsa complex during the mid-brunhes interval. Quat. Sci. Rev. 321, 108375.
Gradstein, F.M., Ogg, G.M., 2020. Geologic Time Scale 2020. Elsevier BV, Amsterdam.
Henrich, R., Baumann, K.-H., 1994. Evolution of the Norwegian current and the Scandinavian ice sheets during the past 2.6 my: evidence from ODP leg 104 biogenic carbonate and terrigenous records. Palaeogeogr. Palaeoclimatol. Palaeoecol. 108, 75–94.
Hillaire-Marcel, C., Ghaleb, B., De Vernal, A., Maccali, J., Cuny, K., Jacobel, A., Le Duc, C., McManus, J., 2017. A new chronology of late Quaternary sequences from the central Arctic Ocean based on "extinction ages" of their excesses in 231Pa and 230Th. G-cubed 18, 4573–4585.
Hodell, D.A., Channell, J.E., Curtis, J.H., Romero, O.E., Röhl, U., 2008. Onset of "Hudson Strait" heinrich events in the eastern north Atlantic at the end of the middle Pleistocene transition (~ 640 ka)? Paleoceanography 23.
Huber, R., Meggers, H., Baumann, K.H., Henrich, R., 2000. Recent and Pleistocene carbonate dissolution in sediments of the Norwegian–Greenland Sea. Mar. Geol. 165, 123–136.
IPCC, 2023. Climate change 2023: synthesis report. In: Lee, H., Romero, J. (Eds.), Contribution of Working Groups I, II and III to the Sixth Assessment Report of the Intergovernmental Panel on Climate Change [Core Writing Team. IPCC, Geneva, Switzerland, pp. 35–115. https://doi.org/10.59327/IPCC/AR6-9789291691647.
Jackson, R., Frederichs, T., Schulz, H., Kucera, M., 2023. Chronology of detrital carbonate events in Baffin Bay reveals different timing but similar average recurrence time of North American-Arctic and Laurentide ice sheet collapse events during MIS 3. Earth Planet Sci. Lett. 613, 118191.
Jin, X., Ma, W., Liu, C., 2022. Origin of the long-term increase in coccolith size and its implication for carbon cycle and climate over the past 2 myr. Quat. Sci. Rev. 290, 107642.
Jutterström, S., Anderson, L.G., 2005. The saturation of calcite and aragonite in the Arctic Ocean. Mar. Chem. 94, 101–110.
Knies, J., O'Regan, M., Marcel, C.H., 2025. Finding Consensus on Arctic Ocean climate history understanding the effects of a "blue" Arctic Ocean on future climate requires a coordinated effort to study. Earth Past Warm Period. Using Vari. Class. Cutt.-edge Method.
Lawrence, D.M., Slater, A.G., Tomas, R.A., Holland, M.M., Deser, C., 2008. Accelerated arctic land warming and permafrost degradation during rapid sea ice loss. Geophys. Res. Lett. 35.
Lisiecki, L.E., Raymo, M.E., 2005. A pliocene-pleistocene stack of 57 globally distributed benthic δ18O records. Paleoceanography 20.
Lucchi, R.G., Camerlenghi, A., Rebesco, M., Colmenero-Hidalgo, E., Sierro, F.J., Sagnotti, L., Urgeles, R., Melis, R., Morigi, C., Bárcena, M.A., Giorgetti, G., Villa, G., Persico, D., Flores, J.A., Rigual-Hernández, A.S., Pedrosa, M.T., Macri, P., Caburlotto, A., 2013. Postglacial sedimentary processes on the Storfjorden and Kveithola trough mouth fans: significance of extreme glacimarine sedimentation. Global Planet. Change 111, 309–326.
Lucchi, R.G., St. John, K.E.K., Ronge, T.A., Barcena, M.A., De Schepper, S., Duxbury, L.C., Gebhardt, A.C., Gonzalez-Lanchas, A., Goss, G., Greco, N.M., Gruetzner, J., Haygood, L., Husum, K., Iizuka, M., Kapuge, A.K.I.U., Lam, A.R., Libman-Roshal, O., Liu, Y., Monito, L.R., Reilly, B.T., Rosenthal, Y., Sakai, Y., Sijinkumar, A.V., Suganuma, Y., Zhong, Y., 2026. And the expedition 403 scientists, Eastern fram Strait paleo-archive. Sites U1621–U1623. In: Lucchi, R.G., St. John, K.E.K., Ronge, T. A. (Eds.), Proceedings of the International Ocean Discovery Program, vol 403. International Ocean Discovery Program, College Station, TX. https://doi.org/10.14379/iodp.proc.403.106.2026.
Marino, M., Maiorano, P., Flower, B.P., 2011. Calcareous nannofossil changes during the mid-pleistocene revolution: paleoecologic and paleoceanographic evidence from north Atlantic site 980/981. Palaeogeogr. Palaeoclimatol. Palaeoecol. 306, 58–69.
Martini, E., 1971. Standard tertiary and Quaternary calcareous nannoplankton zonation. In: Proceedings Second Planktonic Conference, Rome, pp. 739–785.
Matul, A., Spielhagen, R.F., Kazarina, G., Kruglikova, S., Dmitrenko, O., Mohan, R., 2018. Warm-water events in the eastern fram strait during the last 2000 years as revealed by different microfossil groups. Polar Res. 37, 1540243.
Miller, G.H., Alley, R.B., Brigham-Grette, J., Fitzpatrick, J.J., Polyak, L., Serreze, M.C., White, J.W., 2010. Arctic amplification: can the past constrain the future? Quat. Sci. Rev. 29, 1779–1790.
Milliman, J., Troy, P., Balch, W., Adams, A., Li, Y.-H., Mackenzie, F., 1999. Biologically mediated dissolution of calcium carbonate above the chemical lysocline? Deep Sea Res. Oceanogr. Res. Pap. 46, 1653–1669.
Nowaczyk, N.R., Baumann, M., 1992. Combined high-resolution magnetostratigraphy and nannofossil biostratigraphy for late Quaternary Arctic Ocean sediments. Deep-Sea Res., Part A 39, S567–S601.
O'Regan, M., King, J., Backman, J., Jakobsson, M., Pälike, H., Moran, K., Heil, C., Sakamoto, T., Cronin, T.M., Jordan, R.W., 2008. Constraints on the Pleistocene chronology of sediments from the Lomonosov Ridge. Paleoceanography 23.
O'Regan, M., Backman, J., Fornaciari, E., Jakobsson, M., West, G., 2020. Calcareous nannofossils anchor chronologies for Arctic Ocean sediments back to 500 ka. Geology 48, 1115–1119.

Oziel, L., Baudena, A., Ardyna, M., Massicotte, P., Randelhoff, A., Sallée, J.-B., Ingvaldsen, R.B., Devred, E., Babin, M., 2020. Faster Atlantic currents drive poleward expansion of temperate phytoplankton in the Arctic Ocean. Nat. Commun. 11, 1705.
Raffi, I., 2002. Revision of the early-middle Pleistocene calcareous nannofossil biochronology (1.75–0.85 Ma). Mar. Micropaleontol. 45, 25–55.
Raffi, I., Backman, J., 2022. The role of calcareous nannofossils in building age models for Cenozoic marine sediments: a review. Rendiconti Lincei. Sci. Fis. Nat. 33, 25–38.
Raffi, I., Backman, J., Fornaciari, E., Pälike, H., Rio, D., Lourens, L., Hilgen, F., 2006. A review of calcareous nannofossil astrobiochronology encompassing the past 25 million years. Quat. Sci. Rev. 25, 3113–3137.
Razmjooei, M.J., Henderiks, J., Coxall, H.K., Baumann, K.-H., Vermassen, F., Jakobsson, M., Niessen, F., O'Regan, M., 2023. Revision of the Quaternary calcareous nannofossil biochronology of Arctic Ocean sediments. Quat. Sci. Rev. 321, 108382.
Rickaby, R.E.M., Bard, E., Sonzogni, C., Rostek, F., Beaufort, L., Barker, S., Rees, G., Schrag, D.P., 2007. Coccolith chemistry reveals secular variations in the global ocean carbon cycle? Earth Planet Sci. Lett. 253, 83–95.
Rudels, B., Meyer, R., Fahrbach, E., Ivanov, V.V., Østerhus, S., Quadfasel, D., Schauer, U., Tverberg, V., Woodgate, R.A., 2000. Water mass distribution in Fram Strait and over the Yermak Plateau in summer 1997. Ann. Geophys. 18, 687–705.
Saavedra-Pellitero, M., Baumann, K.H., Lamy, F., Köhler, P., 2017. Coccolithophore variability across Marine Isotope Stage 11 in the Pacific sector of the Southern Ocean and its potential impact on the carbon cycle. Paleoceanography 32, 864–880.
Samtleben, C., Schröder, A., 1992. Living coccolithophore communities in the Norwegian-Greenland Sea and their record in sediments. Mar. Micropaleontol. 19, 333–354.
Sato, T., Chiyonobu, S., Hodell, D.A., 2009. Data report: quaternary calcareous nannofossil datums and biochronology in the North Atlantic Ocean, IODP site U1308. Channell, JET, Kanamatsu, T., Sato, T., Stein, R., Alvarez Zarikian, CA, Malone, MJ, Exped. 303, 306.
Seidov, D., Antonov, J.I., Arzayus, K.M., Baranova, O.K., Biddle, M., Boyer, T.P., Johnson, D.R., Mishonov, A.V., Paver, C., Zweng, M.M., 2015. Oceanography north of 60 N from World Ocean database. Prog. Oceanogr. 132, 153–173.
Serreze, M.C., Barrett, A.P., Stroeve, J.C., Kindig, D.N., Holland, M.M., 2009. The emergence of surface-based Arctic amplification. Cryosphere 3, 11–19.
Shackleton, N.J., Opdyke, N.D., 1973. Oxygen isotope and palaeomagnetic stratigraphy of Equatorial Pacific core V28-238: oxygen isotope temperatures and ice volumes on a 105 year and 106 year scale. Quat. Res. 3, 39–55.
Shu, Q., Wang, Q., Årthun, M., Wang, S., Song, Z., Zhang, M., Qiao, F., 2022. Arctic Ocean amplification in a warming climate in CMIP6 models. Sci. Adv. 8 eabn9755.
Silva, A., Palma, S., Moita, M., 2008. Coccolithophores in the upwelling waters of Portugal: four years of weekly distribution in Lisbon bay. Cont. Shelf Res. 28, 2601–2613.
Stöckli, R., Vermote, E., Saleous, N., Simmon, R., Herring, D., 2005. The blue marble next Generation-A true color earth dataset including seasonal dynamics from MODIS. Earth Observ. Published by the NASA.
Thierstein, H., Geitzenauer, K., Molfino, B., Shackleton, N., 1977. Global synchroneity of late Quaternary coccolith datum levels validation by oxygen isotopes. Geology 5, 400–404.
Tyrrell, T., Merico, A., 2004. Emiliania huxleyi: bloom observations and the conditions that induce them. Coccolithophores: from Molecular Processes to Global Impact. Springer, pp. 75–97.
Walczowski, W., Piechura, J., 2011. Influence of the West Spitsbergen current on the local climate. Int. J. Climatol. 31, 1088–1093.
Wei, W., 1993. Calibration of upper pliocene-lower Pleistocene nannofossil events with oxygen isotope stratigraphy. Paleoceanography 8, 85–99.
Wiers, S., Snowball, I., O'Regan, M., Almqvist, B., 2019. Late Pleistocene chronology of sediments from the yermak Plateau and uncertainty in dating based on geomagnetic excursions. G-cubed 20, 3289–3310.
Witte, W.K., Kent, D.V., 1988. Revised magnetostratigraphies confirm low sedimentation rates in Arctic Ocean cores. Quat. Res. 29, 43–53.
Xuan, C., Channell, J.E.T., Polyak, L., Darby, D.A., 2012. Paleomagnetism of Quaternary sediments from Lomonosov Ridge and Yermak Plateau: implications for age models in the Arctic Ocean. Quat. Sci. Rev. 32, 48–63.
Yin, Q., Berger, A., 2010. Insolation and CO2 contribution to the interglacial climate before and after the Mid-Brunhes event. Nat. Geosci. 3, 243–246.
Young, J., Geisen, M., Cros, L., Kleijne, A., Sprengel, C., Probert, I., Østergaard, J., 2003. A guide to extant coccolithophore taxonomy. J. Nannoplankt. Res. Spec. Issue 1, 1–132.
Ziveri, P., Thunell, R.C., Rio, D., 1995. Export production of coccolithophores in an upwelling region: results from San Pedro Basin, Southern California Borderlands. Mar. Micropaleontol. 24, 335–358.
Young, J.R., Bown, P.R. & Lees, J.A. 2026. Nannotax3 website. International Nannoplankton Association. Accessed 20 Jan 2026. URL: *https://www.mikrotax.org/Nannotax3/*.